THREE DIMENSIONALITY IN THE NEAR FIELD OF A ROUND JET

Bharathram Ganapathisubramani
Department of Aerospace Engineering & Mechanics, University of Minnesota
107 Akerman Hall, 110 Union Street SE, Minneapolis, MN – 55455, USA
bugs@aem.umn.edu

Arnauld Loyer
Department of Fluid and Transfer Dynamics, Ecole Centrale de Nantes
BP 92101,F-44321 Nantes Cedex 3, FRANCE
aloyer@atthis.com

Ellen K. Longmire
Department of Aerospace Engineering & Mechanics, University of Minnesota
107 Akerman Hall, 110 Union Street SE, Minneapolis, MN – 55455, USA
ellen@aem.umn.edu

Ivan Marusic
Department of Aerospace Engineering & Mechanics, University of Minnesota
107 Akerman Hall, 110 Union Street SE, Minneapolis, MN – 55455, USA
marusic@aem.umn.edu

ABSTRACT

A round air jet (Re = 16000) was studied using Stereo PIV techniques to understand the characteristics of all three velocity components in the developing shear layer and to study the evolution of three dimensionality with increasing axial distance. Pulsed laser sheets were aligned to illuminate the centerline plane of the jet. The stereo PIV setup was suitably calibrated to translate the resulting pixel displacements into axial, radial, and azimuthal velocity components. The RMS of the azimuthal velocity is of the order of $0.1V_o$ in the shear layer downstream of Y/D ~ 0.5. This is significantly earlier than reported in previous studies. Individual fields show that both vortex cores and braids are three dimensional. However, the initial azimuthal perturbations typically were associated with straining regions immediately upstream of the first vortex ring that formed.

INTRODUCTION

Round jets have been the focus of numerous experimental and numerical studies in the past. Considerable effort has been invested in this field to understand the evolution and the dynamics of the flow structure. Past experimental studies (e.g. Crow and Champagne 1971,Yule 1978) have established that the vorticity layer leaving the nozzle of the jet becomes unstable forming Kelvin-Helmholtz waves and then rolls up into vortex rings that are carried downstream where they become three-dimensional and eventually break down.

In addition to vortex rings, there is significant evidence (e.g. Becker and Masaro 1968, Agui and Hesselink 1988,Yule 1978) of streamwise structures, near both vortex cores and braids. Experiments by Lasheras, Cho & Maxworthy (1986) and numerical computations by Martin and Meiburg (1991) illustrate the role of shearing forces acting perpendicular to the jet axis, in the evolution of streamwise vorticity in the braid region. The experiments of Liepmann & Gharib (1992) which examined planes normal to the axis of a water jet with Re = 5500, indicate that three dimensionality first developed in the braid regions. Streamwise vortices were also observed in a high Reynolds number jet (Re = 78,000) by Paschereit et al. (1992). Also, ina recent study by Citriniti & George (2000) partial velocity field reconstruction od experimental data using POD indicated the presence of counter rotating streamwise vortex pairs in the braid region between successive cores in a jet at Re = 80,000.

Previous experimental studies have not had the capability of obtaining all three velocity components simultaneously in order to correlate and investigate the role of streamwise vorticity and the origin of three dimensionality in the near field of jets. Our primary objective is to study the evolution of three-dimensionality with increasing axial distance and the role of streamwise vorticity in the evolution of three-dimensionality in the flow. This paper reports on Stereo PIV results obtained in the centerline plane of a round air jet. The resulting 3-D velocity vector fields were used to compute the in-plane gradients of the velocity components to investigate streamwise vorticity and its existence in various regions of the flow.

EXPERIMENTAL FACILITY

A sketch jet facility that was used is shown in figure (1). The jet is driven by a six-blade fan, which
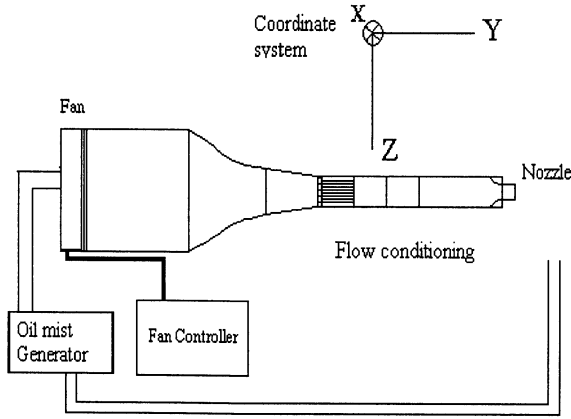

figure 1:   Jet facility

in turn is powered by a standard DC power supply. The flow initially passes through a contraction and flow conditioning consisting of screens and honeycomb. The flow then passes through a second contraction and exits a nozzle with diameter (D) of 30 mm. The second contraction follows a fifth order polynomial curve. Both the jet and the ambient are seeded with olive oil droplets of size ~ 1μm. The olive oil droplets are generated using Laskin nozzles and released just upstream of the fan as shown in figure (1). The ambient is seeded shortly before data acquisition. Hot-wire measurements near the jet exit reveal a top hat profile and a centerline RMS velocity of less than 1% of the mean axial velocity (V_o). Spectral measurements in the jet core show that the flow is not forced.

Two pulsed Nd-YAG lasers were used to illuminate the centerline plane of the jet flow. A spherical bi-convex lens of focal length 1m and a plano-concave cylindrical lens of focal length –25 mm were used to convert each laser beam into a sheet. Two Kodak Megaplus cameras (1024 x 1024 pixels) captured the images. As shown in figure (2), the cameras were oriented at angle 'θ' with respect to the perpendicular from the center of the laser sheet. In this experiment the angle 'θ' was fixed at 30° for both cameras.

STEREO PIV METHOD

In this experiment we used the angular–displacement stereo PIV method in which the cameras are rotated inwards such that their axes intersect at the midpoint of the domain to be recorded as shown in figure (2). Since the object plane is not parallel to the lens plane, there is geometric distortion due to the perspective view.
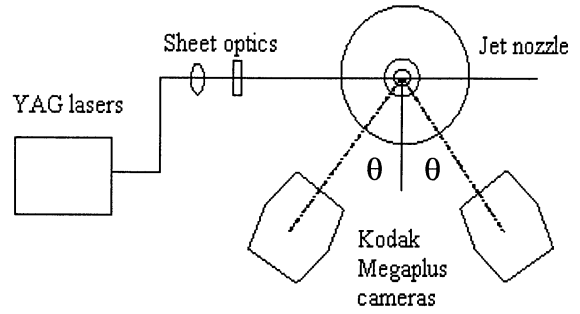

Figure 2:   Experimental setup

Therefore it becomes more difficult to obtain particle images that are well focused across the image plane. To overcome this problem the Scheimpflug condition that requires the object, the lens and the image planes to intersect at a common line, was enforced. This arrangement however introduces a strong perspective distortion and the magnification factor varies across the image plane. These issues can be overcome by calibrating the configuration.

Calibration

The Stereo PIV configuration was calibrated using a fixed grid (figure 3) that contains marker points with alternate points located in different planes. The two planes are separated by 1 mm. This target was aligned with the laser sheet that illuminated the flow field. The cross mark at the center of the image, acts as a reference point for position. The image of the calibration target is captured by both cameras and analyzed. The result of the analysis is a calibration file with a record of the image pixel location (x,y) and target marker location (X,Y,Z) for each marker in the image. Using these points, a set of mapping functions is generated for each camera:

$$x_{left} = f(X,Y,Z) \qquad x_{right} = f(X,Y,Z)$$

$$y_{left} = f(X,Y,Z) \qquad y_{right} = f(X,Y,Z) \, ,$$

where 'f' is the generated mapping function. This set of mapping functions is used to compute the local displacements in seeded flow. After calibration, images are acquired, and an in-plane cross-correlation algorithm computes the relevant pixel displacements for each camera. The following set of transformation equations is used to obtain the fluid displacements:

$$dx_{left} = dX_{fluid}(\delta x_{left}/\delta X) + dY_{fluid}(\delta x_{left}/\delta Y) + dZ_{fluid}(\delta x_{left}/\delta Z)$$

$$dy_{left} = dX_{fluid}(\delta y_{left}/\delta X) + dY_{fluid}(\delta y_{left}/\delta Y) + dZ_{fluid}(\delta y_{left}/\delta Z)$$

$$dx_{right} = dX_{fluid}(\delta x_{right}/\delta X) + dY_{fluid}(\delta x_{right}/\delta Y) + dZ_{fluid}(\delta x_{right}/\delta Z)$$

$$dy_{right} = dX_{fluid}(\delta y_{right}/\delta X) + dY_{fluid}(\delta y_{right}/\delta Y) + dZ_{fluid}(\delta y_{right}/\delta Z) \, ,$$

where (dx_{left}, dy_{left}) and (dx_{right}, dy_{right}) are the pixel displacements from cross-correlation, and (dX,dY,dZ) are the unknown fluid displacements.
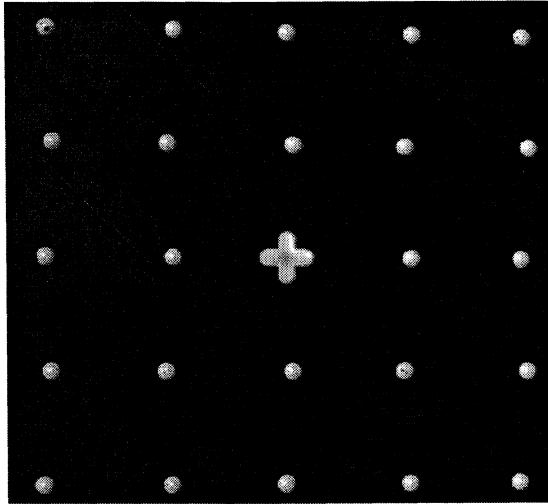
Figure 3:Calibration target as seen by the left camera

The coefficient within the parentheses, displacement gradients with respect to the fluid space, are obtained from the mapping functions generated by calibration. This system of four equations with three variables is solved using the least square method.

To obtain a 3-D vector field with more than 95% valid vectors, it is imperative that the calibration is of very high quality. The two cameras must be focussed at the same plane and location and the system should not experience any kind of physical disturbance between the calibration process and data acquisition. The calibration coefficients and the mapping functions were computed using TSI *Pivcalib* software. A TSI Laser pulse synchronizer box was used to control the strobing and timing of the cameras and the lasers. This box was controlled by TSI *Insight (3.2)* software. The same software also computed pixel and fluid displacements.

Sources of Uncertainty

The major sources of uncertainty in computing the velocity vectors were bias due to correlation calculations and peak fitting and bias generated in curve fitting. Uncertainty in the cross-correlation peak location algorithm depends on pixel displacement, Interrogation spot size, presence of displacement gradients within the spot etc. In this experiment the interrogation spots were 32x32 pixels with 50% overlap, and the magnification was about 5 μm/pixel. In general, displacement uncertainties were of the order of ±0.1 pixels for the Gaussian peak finding algorithm. The resulting uncertainty at all points was less than 1% of the jet exit velocity.

Bias error arises due to the curve fit resulting from the system of four equations in three variables. For a given image set, the calibrated system solution is substituted back into the equations to determine the accuracy of the fit. The difference between the planar pixel displacements calculated by cross-correlation and the pixel displacement obtained by substituting the calibration solution are recorded as 'residual pixels'. The value of the residual is a measure of the

credibility of the 3-D vector field. The residual values were usually highest in regions with strong velocity gradients. This occurs because, the left and right cameras can record different pixel displacements for a single interrogation spot based on their different perspectives. Such differences cause errors in the curve fit when the reconstruction software attempts to match the left and right camera vectors. Plots of residual pixels reveal values, less than 0.1 pixels ($< 0.001V_o$) in the core of the jet and the residues ranging from 0.8–1.5 pixels ($0.08V_o$–$0.15V_o$) in the shear layer, where the velocity gradients affect the reconstruction. Analysis over many image sets indicated that components with larger pixel displacements (streamwise component) contribute significantly to this uncertainty as compared to the component with smaller pixel displacements.

RESULTS AND DISCUSSION

Three dimensional vector fields were computed for more than 300 realizations at various downstream locations. Mean and RMS statistics were computed from ensemble averages of the velocity fields. All computed quantities are made dimensionless using the jet centerline exit velocity $V_o = 9.45$ m/s and jet exit nozzle diameter $D = 30$mm and the corresponding Reynolds number was 16000.

The coordinate system used to describe the results is right handed with the axial direction of the jet being represented by the 'Y' axis (see figure 1). Since the images were taken in the centerline plane of the jet, the X and Z axes are the radial and azimuthal directions respectively. The origin is located at the centerline of the jet exit. The quantities 'V', 'U' and 'W' represent the axial, radial and azimuthal velocity components.

Mean and RMS statistics

The axial mean velocity contours in figure (4) clearly indicate that the core of the jet has a uniform axial velocity distribution and that the shear layer grows with downstream distance. The plot of RMS axial velocity (figure 5) reveals values of nearly 20% in the shear layer and less than 2% in the jet core. Figure(6) show the mean radial velocity component. It is clear from the figure that the radial mean is low in the jet core and it deviates in both directions in the shear layer. Radial mean is positive on the inner side and negative on the outer region of the shear layer and as expected and the turbulent intensity follows the axial velocity behavior. The RMS of the radial velocity is less than 2% in the core of the jet and is more than 10% in the shear layer and increases downstream of y/D = 0.4 reaching a maximum value of about $0.18V_o$ at y/D = 1.7. This is the region where the Kelvin-Helmholtz waves become unstable, resulting in vortex sheet roll up and formation of vortex rings.
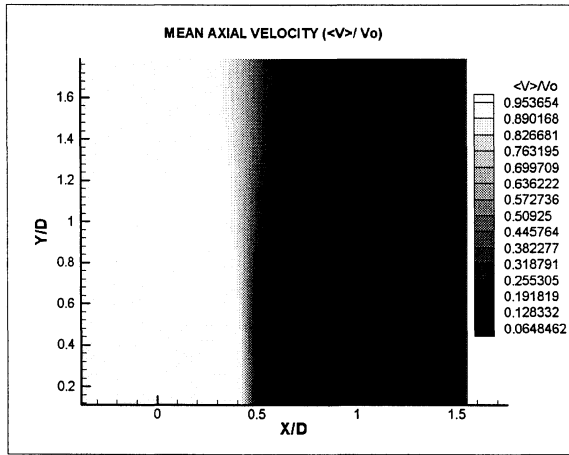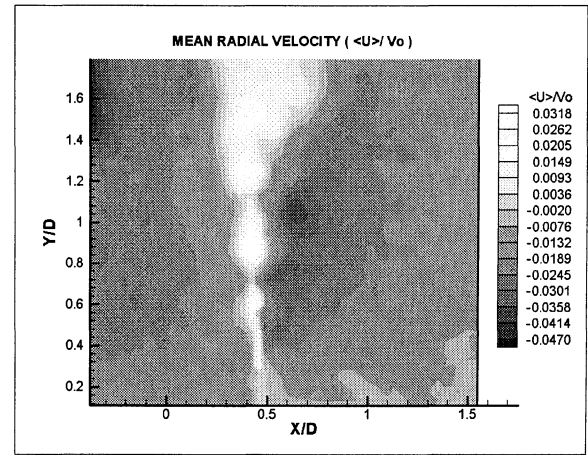
Figure 4:   Mean axial velocity
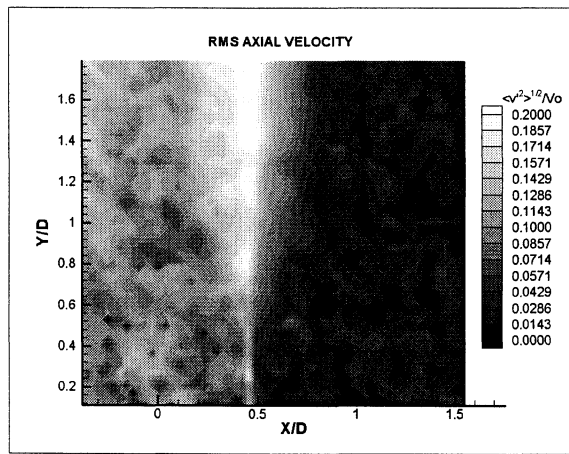

Figure 6:   RMS axial velocity
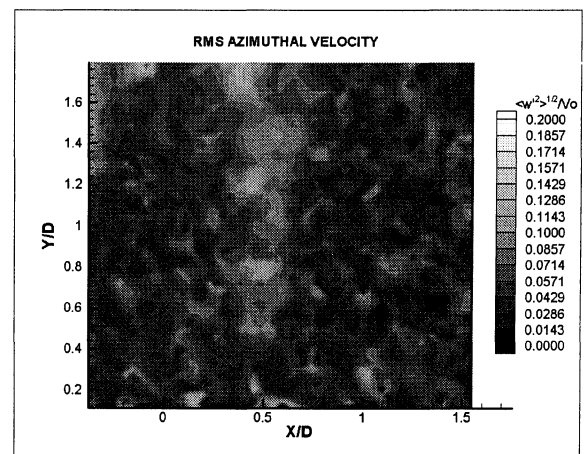

Figure 5:   Mean radial velocity

Figure 7:   RMS azimuthal velocity

The mean and RMS of the azimuthal component were also computed. The mean field revealed that the azimuthal velocity is high in the shear layer and low in the jet core. The RMS of the azimuthal velocity (figure 7) indicates smaller values than those found for the radial and axial components. The RMS values in the shear layer are of the order of $0.1V_o$ downstream of y/D = 0.4 and has a maximum value of $0.13V_o$. A general trend of increasing RMS values with downstream distance is also noticed in all three components.

Vortex Identification

To study the interesting features of the flow and any coexistence of three-dimensionality and azimuthally coherent vortex rings, we need a tool to identify coherent structures. Vortex cores can be identified manually in an image (see figure 8), but to identify them in a velocity field is more challenging. In this paper, we use 'Q', the second invariant of the velocity gradient tensor (Hussain and Jeong 1995)

$$Q = -0.5(S^2 - \Omega^2),$$

where S and Ω are the symmetric and anti-symmetic part of the velocity gradient tensor. However our S and Ω contain only in-plane gradients of the three velocity components. Large positive values of Q suggest the presence of a vortex core and negative values indicate a straining region. The quantity Q was computed for the image set corresponding to figure (8), and the result is given in figure (9).

From this comparison, it can be concluded that the vortex identification parameter Q performs reasonably well at identifying vortex cores as well as the strong straining regions between them.

Three Dimensionality

Using the same image set, the azimuthal velocity (figure 10) and a component of the streamwise vorticity $(\partial W/\partial X)$ (figure 11) were computed. The plot of W demonstrates the degree of three-dimensionality in the near field of the jet. The magnitudes of the azimuthal velocity are of the order of $\pm 0.2V_o$ and $\pm 0.3V_o$ around the vortex cores at y/D = 0.8 and 1.6 respectively. The magnitudes of the azimuthal velocity are large ($0.15V_o - 0.2V_o$) in the straining braid regions between the two vortex
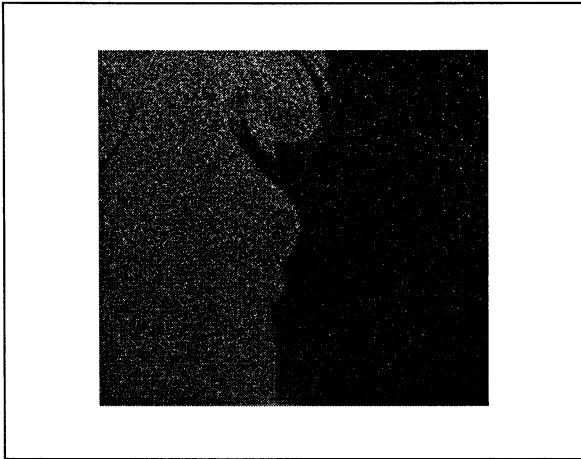
138

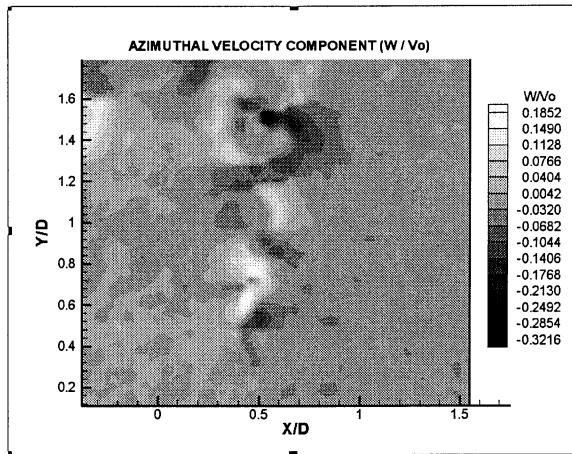Figure 8: Instantaneous image from the left camera
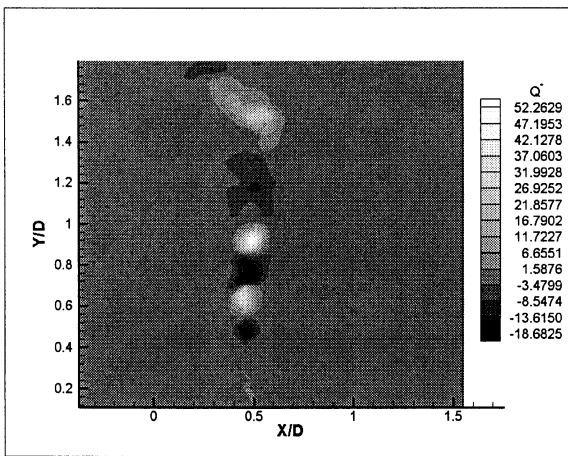

Figure 10:   'W' component

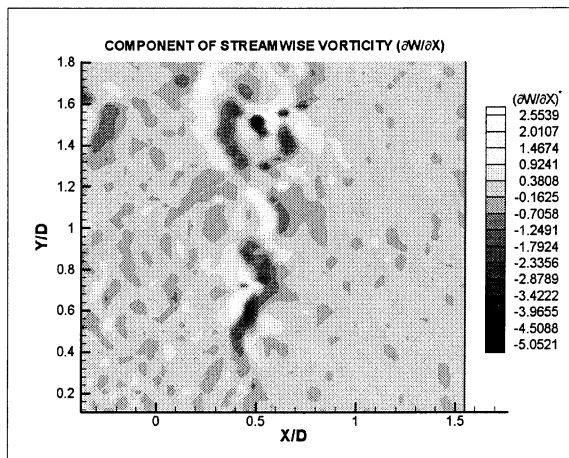Figure 9: Q contour plot for the image

Figure 11: $(\partial W/\partial X)$

cores. Such large magnitudes were not found in previous studies until further downstream. For example, in a jet with Re = 52,000 (Gaydon et al. 1997) a stereo PIV plot normal to the jet axis showed relative magnitudes of the azimuthal velocity similar to those observed in this study at y/D = 2.0. The vortex core has significant positive and negative 'W' indicating either bending of the core or azimuthal swirl within the core. The braid stretching downstream (y/D = 1.0 – 1.4) straddles strong positive and negative strips of W (see figures 9, 10 and 11). The plot of $\partial W/\partial X$ displays a very clear pattern of sign changes surrounding the braid and the vortex cores. This indicates the presence of vortex tubes inclined with respect to the streamwise-radial plane similar to the mushroom pairs observed by Liepmann and Gharib in their flow visualization. Examination of many images indicates that the three-dimensionality and the structural patterns shown here occur very frequently.

Analysis of additional plots of Q and W suggests that the first signs of significant azimuthal velocity appear in the straining region just upstream of the first vortex ring. In this experiment, this region occurs at about y/D ≈ 0.5.

Investigation of velocity fields further downstream illustrates the growth of three-dimensionality. The original vortex cores pair into rings separated by greater axial distances and stronger, longer straining regions (see downstream edge of figure 8 and figures 12 and 13). Note that the straining zone in figure 13 is closely connected to the downstream vortex core but not the upstream one. The plot of azimuthal velocity (figure 14) shows a pair of zones with positive and negative values just upstream of each core center. Typically, these zones have larger size and velocity magnitude than corresponding zones closer to the nozzle exit. The streamwise vorticity component $\partial W/\partial X$ (figure 15) also shows longer strips of greater magnitude than were observed upstream. As before, these strips are oriented at an angle that suggests the existence of streamwise vortex pairs in the braid regions.
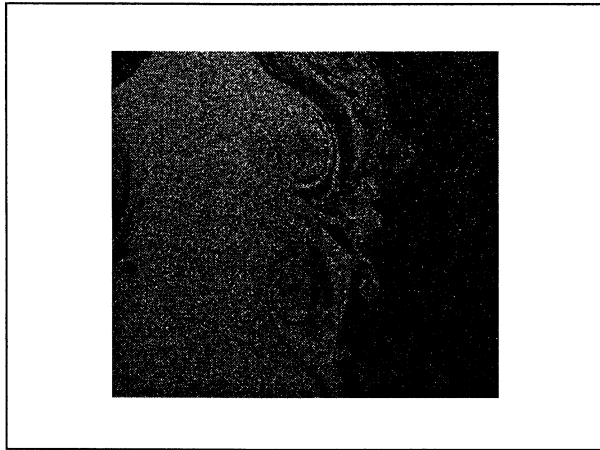
139

Figure 12: Instantaneous image from Left camera

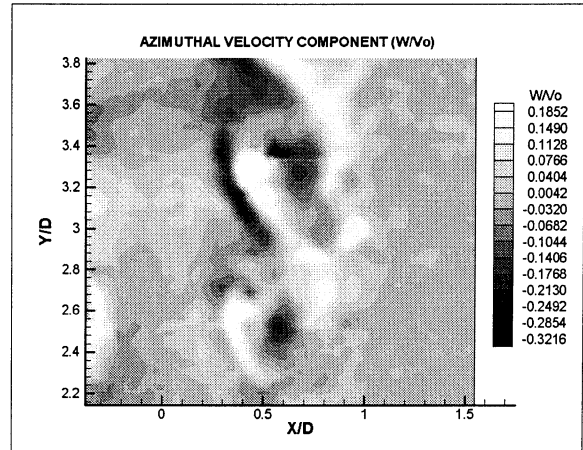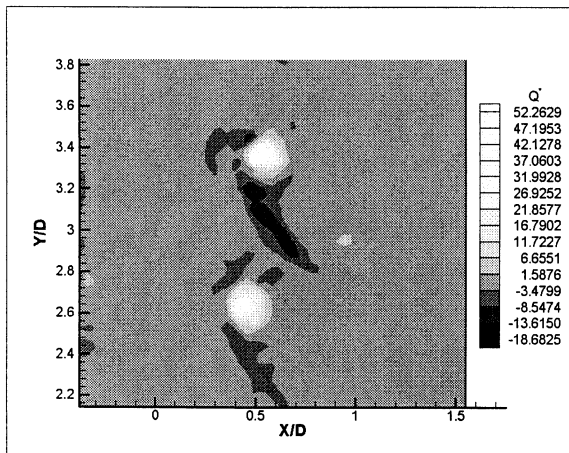Figure 14: 'W' component
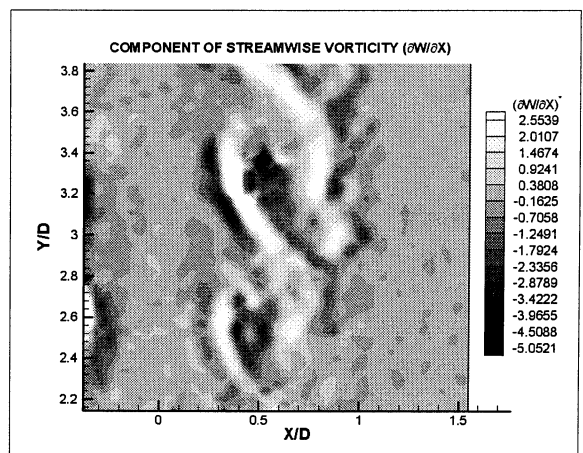

Figure 13: Q contour plot for the image

Figure 15: $(\partial W/\partial X)$

References

Agui, J.C. & Hesselink, L. 1988, Flow visualization and numerical analysis of a coflowing jet: A three dimensional approach. J.Fluid Mech. **191**, pg. 19

Becker,H.A. & Masaro,T.A. 1968, Vortex evolution in a round jet. J.Fluid.Mech **31**, pg. 435

Citriniti, J.H. & George ,W.K. 2000, Reconstruction of global velocity field in the axisymmetric mixing layer utilizing the proper orthogonal decomposition. J.Fluid.Mech **418**, pg. 137

Crow, S.C. & Champagne, F.H. 1971, Orderly structures in jet turbulence. J.Fluid.Mech **48**, pg. 547

M. Gaydon, M. Raffel, C. Willert, M. Rosengarten, and J. Kompenhans 1997, Hybrid stereoscopic particle image velocimetry. Exp. Fluids **23**, pg. 331

Jeong, J. & Hussain, F. 1995, On identification of a vortex. J.Fluid.Mech **285**, pg. 65

Lasheras, J.C., Cho, J.S., & Maxworthy, T. 1986. On the origin and evolution of streamwise vortical structures in a plane free shear-layer. J.Fluid.Mech **172**, pg. 231

Liepmann, D. & Gharib, M. 1992. The role of streamwise vorticity in the near-field entrainment of round jets. J.Fluid.Mech **245**, pg. 643

Martin, J.E. & Meiburg,E. 1991. Numerical investigation of three-dimensionally evolving jet subject to axisymmetric and azimuthal perturbations. J.Fluid.Mech **230**, pg. 271

Paschereit, C. O., Oster, D., Long, T. A., Fiedler, H. E. & Wygnanski, I. 1992 Flow visualization of interactions among large coherent structures in an axisymmetric jet. Exp. Fluids **12**, pg. 189

Yule, A.J. 1978. Large scale structures in the mixing layer of a round jet. J.Fluid.Mech **89**, pg. 413.